© 2023. Published by The Company of Biologists Ltd | Development (2023) 150, dev201341. doi:10.1242/dev.201341

RESEARCH ARTICLE

Single cell evaluation of endocardial *Hand2* gene regulatory networks reveals HAND2-dependent pathways that impact cardiac morphogenesis

Rajani M. George[1,*], Beth A. Firulli[1,*], Ram Podicheti[2], Douglas B. Rusch[2], Brandon J. Mannion[3,4], Len A. Pennacchio[3,4,5], Marco Osterwalder[3,6,7] and Anthony B. Firulli[1,‡]

ABSTRACT

The transcription factor HAND2 plays essential roles during cardiogenesis. *Hand2* endocardial deletion (*H2CKO*) results in tricuspid atresia or double inlet left ventricle with accompanying intraventricular septum defects, hypo-trabeculated ventricles and an increased density of coronary lumens. To understand the regulatory mechanisms of these phenotypes, single cell transcriptome analysis of mouse E11.5 *H2CKO* hearts was performed revealing a number of disrupted endocardial regulatory pathways. Using HAND2 DNA occupancy data, we identify several HAND2-dependent enhancers, including two endothelial enhancers for the shear-stress master regulator KLF2. A 1.8 kb enhancer located 50 kb upstream of the *Klf2* TSS imparts specific endothelial/endocardial expression within the vasculature and endocardium. This enhancer is HAND2-dependent for ventricular endocardium expression but HAND2-independent for *Klf2* vascular and valve expression. Deletion of this *Klf2* enhancer results in reduced *Klf2* expression within ventricular endocardium. These data reveal that HAND2 functions within endocardial gene regulatory networks including shear-stress response.

KEY WORDS: HAND factors, Cardiogenesis, Congenital heart defects, Endocardial development, Mouse

INTRODUCTION

Cardiac morphogenesis is a complex process requiring the synergistic action of multiple tissue types and fine-tuned control of morphogenetic events that are coordinated through the actions of transcription factors within each contributing cell type. Spatial and temporal specific cell signaling between the developing myocardium, the muscular portion of the heart, and endocardium, the inner endothelial lining of the heart, is required for normal cardiogenesis. The embryonic day (E) 12.5 myocardium of the developing ventricles expresses vascular endothelial growth factor A (VEGFA), which signals to the endocardium through its interactions with VEGF receptor 2 (VEGFR2; also known as KDR) to establish the coronary plexus, which will mature to contribute to the coronary arteries (Wu et al., 2012). In the atria, NOTCH signaling initiated within the endocardium communicates with receptors expressed in the myocardium regulating valve and sinoatrial node development (Wang et al., 2020, 2013). Ventricular NOTCH signaling from the endocardium is also required for myocardial BMP10 expression, which is essential for normal trabeculation (Chen et al., 2004; Del Monte-Nieto et al., 2018; Grego-Bessa et al., 2007).

Recent work has revealed that the basic helix loop helix (bHLH) transcription factor HAND2 is required for NOTCH-dependent functions within the endocardium, modulating trabeculation, septation, coronary vascular maturation, as well as endocardial maturation within the embryonic heart (VanDusen et al., 2014a). Conditional endocardial deletion of *Hand2* using *Nfatc1*^{Cre} (*H2CKO*) (VanDusen et al., 2014a; Wu et al., 2012) results in embryonic lethality by E12.5. Embryos exhibit tricuspid atresia (TA) or double inlet left ventricle (DILV), in which both tricuspid and mitral valves connect the atria with the left ventricle (LV) (VanDusen et al., 2014a). *H2CKO*s also exhibit hypoplastic myocardium, an intraventricular septum (IVS) that is shifted to the right generating a smaller right ventricle (RV) and larger LV. *H2CKO* hearts are hypotrabeculated, and occasionally present with multiple IVS (VanDusen et al., 2014a). In addition to these defects, *H2CKO* hearts exhibit a pronounced hypervascularization phenotype with an increased number of coronary arteries within the myocardium (VanDusen et al., 2014a).

To investigate transcriptomic changes within *H2CKO* endocardium, we employed single cell (sc) RNA-seq to identify several gene regulatory networks (GRNs) compromised by HAND2 loss of function. The most notable GRN impacted by the loss of HAND2 is the Apelin Endothelial Signaling Pathway, which is related to shear-stress response. Based on the overlap of significant gene expression changes with established HAND2 DNA occupancy data (Laurent et al., 2017), we sought to identify putative HAND2-dependent endocardial transcriptional enhancers. We selected five genes that showed robust expression changes associated with bound HAND2 to further evaluate: *Igf2*, *Igf2R*, *Ptn*, *Tmem108* and *Klf2*. Putative enhancer sequences for two of the selected genes, *Igf2R* and the shear-stress master regulator gene *Klf2*, exhibited functional endocardial/endothelial transcriptional enhancers via F0 transgenic reporter analysis. We further characterized the activity of a 1.8 kb *Klf2* enhancer located −50 kb upstream of the *Klf2* transcriptional start site (TSS). We observed that the −50 kb *Klf2* enhancer is

[1]Herman B Wells Center for Pediatric Research, Departments of Pediatrics, Anatomy and Medical and Molecular Genetics, Indiana Medical School, Indianapolis, IN 46202, USA. [2]Center for Genomics and Bioinformatics, Indiana University, Bloomington, IN 47405, USA. [3]Environmental Genomics and Systems Biology Division, Lawrence Berkeley National Laboratory, Berkeley, CA 94720, USA. [4]Comparative Biochemistry Program, University of California, Berkeley, CA 94720, USA. [5]US Department of Energy Joint Genome Institute, Lawrence Berkeley National Laboratory, Berkeley, CA 94720, USA. [6]Department for BioMedical Research (DBMR), University of Bern, Bern 3008, Switzerland. [7]Department of Cardiology, Bern University Hospital, Bern 3010, Switzerland.
*These authors contributed equally to this work

‡Author for correspondence (tfirulli@iu.edu)

R.M.G., 0000-0002-9153-5523; B.A.F., 0000-0001-6687-8949; B.J.M., 0000-0002-1149-3790; M.O., 0000-0002-1969-2313; A.B.F., 0000-0001-6687-8949

Handling Editor: Benoit Bruneau
Received 30 September 2022; Accepted 26 December 2022

Development (2023) 150, dev201341. doi:10.1242/dev.201341

active within the early developing vasculature endothelium and, importantly, within the endocardium, recapitulating the endogenous *Klf2* expression pattern. To determine whether HAND2 is necessary for *Klf2* enhancer endocardial expression *in vivo*, we interrogated the activity of the −50 kb *Klf2* enhancer on the *H2CKO* background. Indeed, our data revealed that, in the absence of HAND2, activity of the −50 kb *Klf2* enhancer is robustly reduced within trabecular endocardium but is unaffected within the systemic vasculature and developing valves. Gene edited deletion of the −50 kb *Klf2* [$Klf2^{\Delta\text{-}50:(3.9kb)/\Delta\text{-}50:(3.9kb)}$] enhancer demonstrated its requirement for *Klf2* endocardial expression. Collectively, these findings demonstrate several previously unreported endocardial HAND2-dependent gene regulatory pathways, including the shear-stress response pathway, mediated in part through HAND2 regulation of *Klf2*.

RESULTS

Deletion of *Hand2* results in disruption of a number of endocardial GRNs, including the shear-stress pathway

To further investigate the role of HAND2 within the developing endocardium, we crossed *Hand2*-conditional mice ($H2^{fx/fx}$; $R26R^{mTmG/mTmG}$) (Morikawa et al., 2007; Muzumdar et al., 2007) with the endocardial-specific $Nfatc1^{Cre}$ (Wu et al., 2012) to generate *H2CKO* ($Nfatc1^{Cre}Hand2^{fx/fx}R26R^{mTmG/wt}$) as well as control littermates ($Hand2^{fx/+}R26R^{mTmG/wt}$) and isolated E11.5 hearts for scRNA-seq analysis using the 10x Genomics platform. In *H2CKO* hearts, Cre-recombinase mediated recombination led to switching of tdtomato epifluorescence to GFP epifluorescence, which allowed for the quick identification of Cre-positive embryos. Rapid PCR genotyping was used to identify the *Hand2*-conditional allele status of the embryos. We sequenced 13,885 unique barcodes from a single *H2CKO* heart, and 14,259 barcodes from a single control heart. Based on the high expression of hemoglobin genes, we excluded 5828 barcodes from *H2CKO* and 3150 barcodes from control hearts. Next, we excluded barcodes where the total number of genes was greater than 2500 (indicating multiplets) from the analysis. The remaining 6232 barcodes from *H2CKO* and 5408 barcodes from control hearts were used for further analysis. Non-linear dimensionality reduction using uniform manifold approximation and projection (UMAP) plots resulted in 13 transcriptionally distinct clusters (Fig. 1A; Table S1). Fig. S1 displays control and *H2CKO* cells mapped separately.

Cluster identity was assigned by comparing gene expression of a gene in the control cluster against expression of the same gene in all other control clusters combined at a threshold of 0.25 log2FC, which establishes a rigorous threshold for significance (Table S1). Clusters 0 (red) and 1 (pink) represented 2793 cells, exhibited similar transcriptional profiles and expressed the following cardiomyocyte marker gene transcripts: *Myh6* (99.4% cells in cluster 0, 98.1% cells in cluster 1), coding for alpha myosin heavy chain (αMHC), and actinin alpha 2 (*Actn2*; 99.9% of cells in clusters 0 and 1; Fig. 1A; Fig. S2; Table S1). The 1030 cells within cluster 2 (brown) expressed the extracellular matrix protein coding gene periostin (*Postn*, 99.8% of cells), the bHLH transcription factor gene *Twist1* (99.1% of cells), the matricellular protein coding gene transforming growth factor beta induced (*Tgfbi*, 98% of cells) and represent atrioventricular (AV) cushion cells that have undergone endothelial-to-mesenchymal transition (EMT, Fig. S2; Table S1). Cluster 3 (orange) consisted of 993 cells that were identified as outflow tract mesenchyme based on the expression of the neurovascular guiding factor semaphorin 3c (87% of cells) and bone morphogenetic protein 4 (*Bmp4*, 88% of cells; Fig. S2; Table S1). Clusters 4 (light purple; 740 cells) and 5 (dark purple; 686 cells) consisted of cardiac neural crest cells as determined by the expression of *Twist1* (99.8% of cells in cluster 4, 100% in cluster 5), insulin growth factor (*Igf1*, 98% of cells in both clusters), and high mobility group transcription factor *Sox9* (94% of cells in cluster 4 and 96% of cells in cluster 5, Fig. S2; Table S1). The 594 cells in cluster 6 consisted of epicardial cells (light green), undergoing transition to a fibroblast phenotype as marked by the expression of the growth factor pleiotrophin (*Ptn*, 100% of cells), T-box transcription factor *Tbx18* (90% of cells) and bHLH transcription factor *Tcf21* (98% of cells; Fig. S2; Table S1). Cluster 7 consisted of 564 cells (light blue) that were identified as endocardial cells by the expression of the transmembrane transport protein *Ramp2* (100% of cells), the vascular endothelial cadherin (*Cdh5*, 99% of cells, Fig. S2; Table S1), platelet endothelial cell adhesion molecule (*Pecam1*, 95% of cells), and the nuclear factor of activated T cells (*Nfatc1*, 64% of cells). Cluster 8 consisted of 542 cells and was identified as a second epicardial cell cluster (dark green) expressing *Ptn* (100% of cells), *Tbx18* (97% of cells) and *Tcf21* (97% of cells; Fig. S2; Table S1). Cluster 9 consisted of 462 cells and represented a second endocardial cell cluster (dark blue) expressing *Ramp2* (100% of cells), *Cdh5* (95% of cells), *Pecam1* (98% of cells) and *Nfatc1* (88% of cells; Fig. S2; Table S1). Cluster 10 did not express any gene that exhibited a log2 fold change of expression within the cluster and outside the cluster greater than 0.25, thus this cluster (grey) has remained undefined. Cluster 11 represented the conduction system cell cluster (yellow) marked by expression of calcium channel, voltage-dependent, α2/δ2 subunit 2 (*Cacna2d2*, 97% of cells) and calcium channel, voltage-dependent, T type, α 1H subunit, (*Cacna1h*, 65% of cells). Cluster 12 (black) represented the lymphocyte population as indicated by expression of interferon induced transmembrane protein 3 (*Ifitm3*, 47% of cells) and histocompatibility 2, D region locus 1 (*H2-D1*, 93% of cells; Fig. S2; Table S1). *Nfatc1* expression robustly marked both cluster 7 (64% of cells) and cluster 9 (88% of cells; Fig. 1B). Comparison of *H2CKO* and control barcodes specific for *Hand2* expression exhibited robust downregulation within these two endocardial clusters in the presence of $Nfatc1^{Cre}$ (cluster 7 log2FC −1.5, $P=1.5\times10^{-52}$; cluster 9 log2FC −1.66, $P=9.3\times10^{-55}$; Fig. 1B; Fig. S3). Note that cluster 10 (undefined) maintained *Hand2* expression post-deletion (Fig. 1B; Fig. S3).

Analysis of endocardial clusters 7 and 9 indicates misregulation within several endocardial gene regulatory networks

To examine transcriptome data in an unbiased fashion, we employed Ingenuity Pathway Analysis (IPA) on differentially expressed genes (log2FC>±0.5) from *H2CKO* and control cells (Table 1; Fig. S4; Table S2). Loss of *Hand2* within the endocardium led to significant changes in developmental, morphological, and cardiovascular gene regulatory networks (Table 1; Fig. S5). IPA on cluster 7 indicated that *Hand2* is downregulated within the Cardiac Hypertrophy Signaling (Enhanced) canonical pathway (*z*-score −1.807, −log *P*-value 2.8; Table S2), which is close to a significant *z*-score absolute value of 2.

We also observed abnormal expression of a number of endocardial transcripts including endothelin converting enzyme 1 (*Ece1*), a shear-stress responsive gene expressed by vascular endothelial cells and required for formation of patent vasculature in the developing heart (Masatsugu et al., 2003; Robinson et al.,

Development (2023) 150, dev201341. doi:10.1242/dev.201341

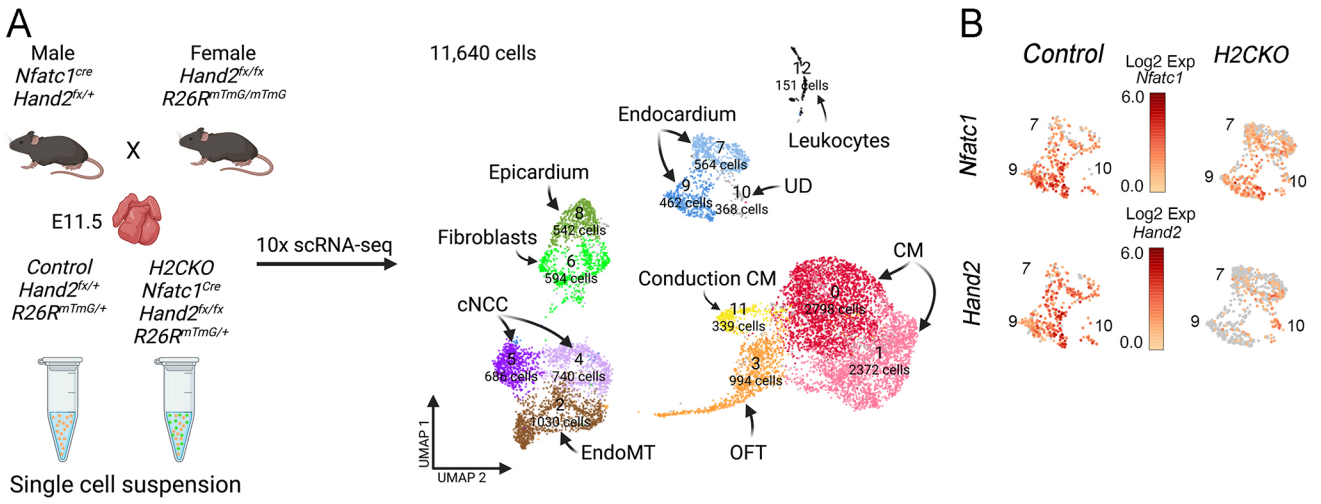

Fig. 1. scRNA-seq analysis of *Nfatc1*^{cre} *Hand2*$^{fx/fx}$ E11.5 ventricles. (A) Experimental design (left) and UMAP plot (right) of all barcodes captured with scRNA-seq of E11.5 embryos from control (*Hand2*$^{fx/+}$R262R$^{mTmG/+}$) and *H2CKO* (*Nfatc1*^{cre}*Hand2*$^{fx/fx}$R262R$^{mTmG/+}$) hearts. Control *n*=5408; *H2CKO n*=6232. CM, cardiomyocytes; cNCC, cardiac neural crest cells; EndoMT, endothelial-to-mesenchymal transition; OFT, outflow tract mesenchyme; UD, undefined. (B) Expression of *Hand2* and *Nfatc1* in endocardial clusters 7 and 9 in control and *H2CKO* hearts. Note, *Hand2* is expressed within cluster 10 cells and is not deleted within the *H2CKO* hearts.

2014). *Ece1* was significantly downregulated within *H2CKO* endocardium (cluster 7 log2FC −1.16, P=2.69×10^{-28}; cluster 9 log2FC −0.45, P=9.05×10^{4}; Table S3). Concomitantly, the *Ece1* substrate endothelin 1 (*Edn1*), a potent vasoconstrictor that is secreted by endothelial cells when laminar flow induces shear stress (Morawietz et al., 2000), was upregulated within *H2CKO* endocardium (cluster 7 log2FC 0.58, P=1.9×10^{-9}). Previous work has shown that EDN1 signaling lies upstream of *Hand2* within the cranial neural crest cells during craniofacial morphogenesis (Charité et al., 2001; Clouthier et al., 2000). Thus, the observed increase in *Edn1* could reflect a feedback compensation as the result of the endocardial loss of *Hand2*.

Fibronectin 1 (*Fn1*), a component of the extracellular matrix secreted by endothelial cells, was significantly downregulated within clusters 7 and 9 (cluster 7 log2FC −1.17, P=1.4×10^{-21}; cluster 9 log2FC −0.66, P=1.6×10^{-4}, Table S3). *Fn1* appeared in multiple IPA pathways (Table 1) including: Wound Healing Signaling Pathway (*z*-score −3.606, −log *P*-value 4.67), Pulmonary Fibrosis Idiopathic Signaling Pathway (*z*-score −3.273, −log *P*-value 9.66) and Tumor Microenvironment Pathway (*z*-score −2.449, −log *P*-value 2.1).

Table 1. IPA analysis detailing the top 10% of differentially expressed genes in control versus *H2CKO* populations within cluster 7

Ingenuity canonical pathways	−log(*P*-value)	*Z*-score
Wound healing signaling pathway	4.67	−3.606
Pulmonary fibrosis idiopathic signaling pathway	9.66	−3.273
Pulmonary healing signaling pathway	1.87	−2.646
Tumor microenvironment pathway	2.10	−2.449
NF-κB signaling	0	−2.449
STAT3 pathway	1.54	−2.236
Apelin endothelial signaling pathway	1.47	−2.000
Cardiac hypertrophy signaling (enhanced)	2.80	−1.807
RHOA signaling	4.53	2.333
EIF2 signaling	12.90	2.714

Negative *z*-scores represent downregulated pathways, positive *z*-scores represent upregulated pathways.

The mechanosensitive transcription factor hypoxia inducible factor 1 alpha (*Hif1a*) was significantly downregulated within endocardial clusters (cluster 7 log2FC −0.58, P=4.5×10^{-12}; cluster 9 log2FC −0.48, P=2.3×10^{-10}; Table S3; Feng et al., 2017). IPA analysis revealed that related canonical pathways which included *Hif1a* were disrupted (Table 1; Table S2): Pulmonary Healing Signaling Pathway (*z*-score −2.65, −log *P*-value 1.87) and Tumor Microenvironment Pathway (*z*-score of −2.449, −log *P*-value 2.1). The Tumor Microenvironment Pathway also included *Igf2*, the gene that encodes insulin-like growth factor 2, which was significantly downregulated in *H2CKO* endocardial clusters (cluster 7 log2FC −1.44, P=3.2×10^{-46}; cluster 9 log2FC −1.81, P=2.1×10^{-65}). Indeed, *Hif1a* transcriptionally regulates *Igf2* via hypoxia responsive elements at the *Igf2* locus (Feldser et al., 1999). Within endocardial cells, angiogenesis requires the action of the shear-stress master regulator KLF2 (Nigro et al., 2011).

Given the presence of two endothelial/endocardial clusters and to better understand the differences within these cells, we undertook the direct comparison of gene expression within clusters 7 and 9 between the control and *H2CKO* cell populations (Fig. S6; Table S4). Results showed that 785 genes were differentially expressed between control in clusters 7 and 9. These genes included *Klf2*, (log2FC −0.536095853), *Hey2* (Seya et al., 2021) (log2FC −0.610741244), the NOTCH-dependent ligand *Wnt4* (Luxán et al., 2016) (log2FC −0.857926425) and the endocardial specific *Irx6* (Mummenhoff et al., 2001) (log2FC 0.288606862; Table S4, tab control). Similar analysis on *H2CKO* data revealed that 981 genes were differentially expressed between clusters 7 and 9, including the aforementioned examples (Table S4, tab *H2CKO*). In addition, 501 common genes were differentially regulated between control and *H2CKO* clusters 7 and 9, with 284 genes uniquely regulated in controls and 480 genes uniquely regulated in *H2CKO* (Fig. S6; Table S4, tabs control only and *H2CKO* only). Given that there was not a significant amount of coronary vasculature present at E11.5 (Ivins et al., 2015), it is possible that these two clusters represented distinct populations of maturing endocardium, where cluster 7 cells might contribute to the future coronary vasculature as *H2CKO*

Development (2023) 150, dev201341. doi:10.1242/dev.201341

hearts exhibited hypovascularized ventricles (VanDusen et al., 2014a).

The shear-stress master regulator gene *Klf2* is specifically downregulated within the ventricular portion of the *H2CKO* endocardium

IPA also revealed that *H2CKO* mutants exhibited a significant downregulation of the Apelin Signaling Pathway, with a *z*-score of −2 (−log *P*-value 1.47, Table 1). Apelin is an angiogenic factor that controls migration of endothelial cells and is required for the normal development of blood vessels (Helker et al., 2020; Kwon et al., 2016; Lu et al., 2017). The Apelin Signaling IPA pathway includes a major contributing factor to normal vasculogenesis and ventricular morphogenesis within the embryonic heart – shear-stress signaling (Haack and Abdelilah-Seyfried, 2016). We observed that the gene coding for the shear-stress regulated transmembrane receptor heart of glass (*Heg1*) was significantly downregulated within both endocardial clusters (cluster 7 log2FC −0.36, P=6.35×10^{-9}; cluster 9 log2FC −0.9 P=1×10^{-15}; Table S3). *Heg1* zebrafish mutants exhibit significant vascular malformations (Kleaveland et al., 2009). Interestingly, the transcription factor KLF2 is a direct regulator of *Heg1* expression (Razani et al., 2001; Zhou et al., 2016). KLF2 is a well-studied shear-stress response transcription factor considered the master regulator of this response (Bhattacharya et al., 2005; Chiplunkar et al., 2013; Sangwung et al., 2017).

As the hypervascularization phenotype observed in the *H2CKO* mutants could be caused by defective angiogenesis, and KLF2 is a major regulator of angiogenesis, we employed *in-situ* hybridization to closely examine both *Hand2* and *Klf2* transcripts within E12.5 control and *H2CKO* embryo hearts (Fig. 2). Results showed that *Hand2* expression within the trabecular endocardium of the ventricles was significantly reduced in *H2CKO* hearts when compared with controls (Fig. 2A,C). *Klf2* was also robustly expressed within the ventricular endocardium (Fig. 2B,B′, black arrowheads), and particularly within areas of high shear stress such as the endocardial lining of the AV canal (Fig. 2B′, red arrowheads; Chiplunkar et al., 2013). We observed that *Klf2* expression within the ventricular endocardium of *H2CKO* hearts was greatly reduced; however, *Klf2* expression within the endocardial lining of the AV canal as well as within the systemic vasculature was maintained (Fig. 2D,D′, compare tissues marked by red and black arrows). Next, we examined genes downstream of KLF2 that were significantly changed within *H2CKO* endocardial clusters 7 and 9 (Table S5). Indeed, we observed significant changes in gene expression within KLF2 target genes, which suggested that loss of HAND2 in the endocardium reduced *Klf2* expression as well the expression of *Klf2* target genes (Table S5).

Comparison of scRNA-seq regulation and HAND2 DNA occupancy identifies three novel endothelial/endocardial enhancers

The differential gene expression profiles in endocardial clusters from wild-type (WT) and *H2CKO* hearts suggested a direct interaction of the HAND2 transcription factor with *cis*-regulatory elements in the respective loci for transcriptional control. We selected a subset of genes (*Igf2*, *Tmem108*, *Ptn*, *Igf2R* and *Klf2*) for which distinct HAND2 interaction peaks were identified in the respective regulatory domains by determining regions of evolutionary conservation and HAND2 DNA binding (Fig. 3; Table 2). For identification of HAND2 target regions, we used established E10.5 chromatin immunoprecipitation (ChIP)-seq data from mouse embryonic hearts expressing a *Hand2*^{3xFlag} knock-in

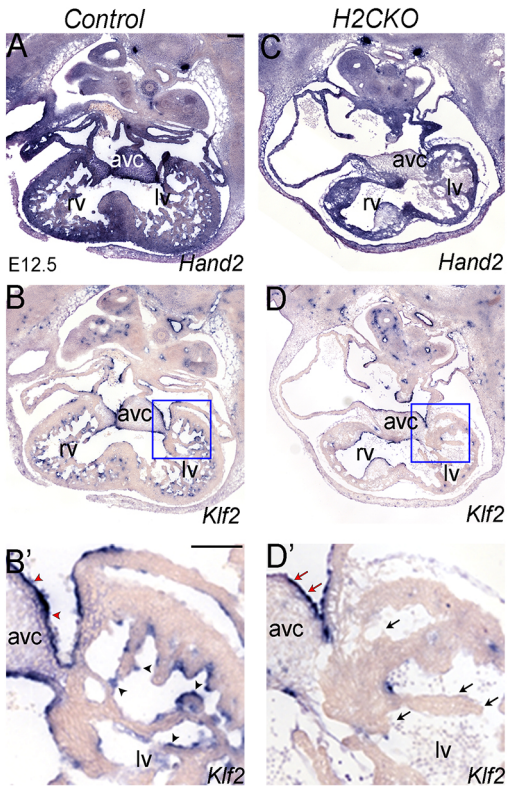

Fig. 2. Expression of *Klf2* in *H2CKO* hearts. (A-B′) Representative *in-situ* hybridization section showing *Hand2* and *Klf2* expression in E12.5 *Hand2*$^{fx/fx}$ controls. Black arrowheads indicate ventricular endocardium. Red arrowheads indicate endocardium covering the AV cushion. n=10. (C-D′). Representative *in-situ* hybridization section showing *Hand2* and *Klf2* expression in E12.5 *Nfatc1*^{cre} *Hand2*$^{fx/fx}$ *H2CKO* hearts. Black arrows indicate ventricular endocardium. Red arrows indicate endocardium covering the AV cushion. avc, atrioventricular canal; lv, left ventricle; rv, right ventricle. Scale bars: 100 µm.

allele (Laurent et al., 2017). To validate and define cardiac *in vivo* activities of putative enhancer regions in the selected subset of gene loci we employed *lacZ* transgenic reporter assays, involving enSERT, a method for CRISPR-mediated site-directed reporter transgenesis targeting the *H11* locus (Kvon et al., 2020; Osterwalder et al., 2022).

Three of our putative HAND2-dependent enhancers that exhibit evolutionary conservation and HAND2 DNA occupancy did not exhibit endocardial/endothelial enhancer activity (Fig. S7). IGF2 is a secreted growth factor expressed within the epicardium and endocardium during heart development (Shen et al., 2015) and is highly downregulated within clusters 7 and 9 in *H2CKO* mutants (Table S3). At the *Igf2* genomic locus, a conserved non-coding element (CNE) located 70 kb 3′ to the coding region (Fig. S7A) showed pronounced HAND2 DNA occupancy. However, analysis by enSERT exhibited no enhancer activity of this element (n=6/9 tandems; Fig. S7B,B′). TMEM108 is implicated as a marker for progenitor epicardial cell populations although its role within the endocardium is currently unclear (Bochmann et al., 2010). *Tmem108* is significantly downregulated within endocardial clusters 7 and 9 (Table S3); however, a HAND2-occupied CNE located 5′ of *Tmem108* exhibited no enhancer activity (n=2/3 tandems; Fig. S7C-D′). *Ptn* codes for a secreted cytokine, is an inducer of EMT, and is mitogenic to endothelial cells, resulting in angiogenesis (Perez-Pinera et al., 2008). *Ptn* is significantly

Development (2023) 150, dev201341. doi:10.1242/dev.201341

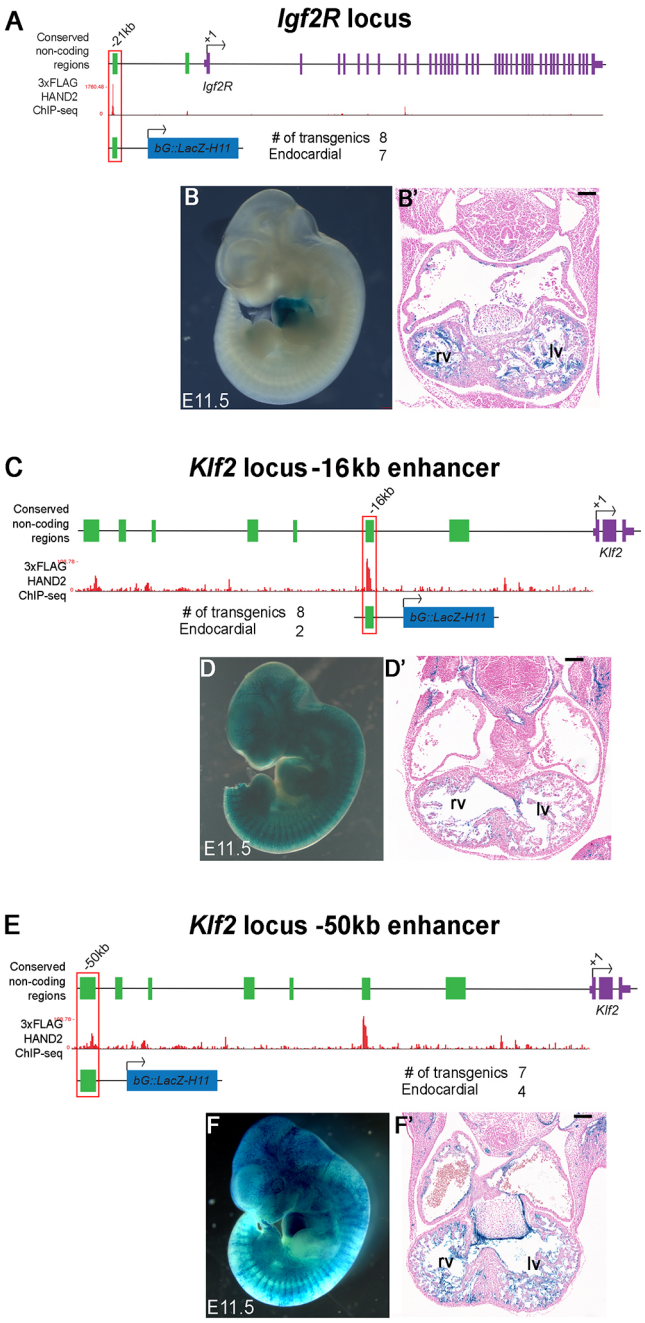

Fig. 3. F0 reporter expression analysis of target genes showing both altered gene expression and HAND2 DNA-occupancy. (A) *Igf2R* genomic locus showing conserved non-coding regions (green solid boxes), TSS (+1), relative location of enhancer element (−21 kb, red outline). *HAND2*^{3xFlag} ChIP-seq data (Laurent et al., 2017) showing genomic regions of HAND2 binding. (B,B′) The −21 kb HAND2 binding conserved non-coding region at *Igf2R* locus used to make transgenic F0 embryos and β-galactosidase staining results. Representative wholemount image of E11.5 transgenic embryo. Number of transgenic F0 embryos obtained=8. Number of F0 embryos that showed endocardial staining=7. (C) *Klf2* genomic locus showing conserved non-coding regions (green solid boxes), TSS (+1), relative location of enhancer element (−16 kb, red outline). *HAND2*^{3xFlag} ChIP-seq data (Laurent et al., 2017) showing genomic regions of HAND2 binding. (D,D′) The −16 kb HAND2 binding conserved non-coding region at *Klf2* locus used to make transgenic F0 embryos and β-galactosidase staining results. Representative whole mount image of E11.5 transgenic embryo. Number of transgenic F0 embryos obtained=8. Number of F0 embryos that showed endothelial/endocardial staining=2. (E) *Klf2* genomic locus showing conserved non-coding regions (green solid boxes), TSS (+1), relative location of enhancer element (−50 kb, red outline). *HAND2*^{3xFlag} ChIP-seq data (Laurent et al., 2017) showing genomic regions of HAND2 binding. (F,F′) The −50 kb HAND2 binding conserved non-coding region at *Klf2* locus used to make transgenic F0 embryos and β-galactosidase staining results. Representative whole mount image of E11.5 transgenic embryo. Number of transgenic F0 embryos obtained=7. Number of F0 embryos that showed endothelial/endocardial staining=4. Scale bars: 100 µm. lv left ventricle, rv right ventricle.

downregulated within both clusters 7 and 9 (Table S3). We tested a HAND2-occupied CNE located 3′ of *Ptn*; however, results showed no E11.5 heart expression (n=2/3 tandems; Fig. S7E-F′).

Three of our putative HAND2-dependent enhancers that exhibited robust HAND2 DNA occupancy also exhibited endocardial/endothelial enhancer activity. We successfully interrogated a HAND2-occupied CNE located 21 kb 5′ of the *Igf2R* TSS (Fig. 3A). *Igf2R* is robustly expressed within the endocardium (Wang et al., 2019) and lacks a tyrosine kinase domain acting as a negative regulator of IGF2 (Braulke, 1999; Ludwig et al., 1996). *Igf2r* was significantly downregulated within *H2CKO* endocardial clusters 7 and 9 (Table S3). EnSERT analysis of the *Igf2R* HAND2-occupied CNE resulted in 7/8 transgenic embryos (n=5 tandems) with cardiac-specific *lacZ* staining at E11.5, including the endocardium, thus uncovering a novel endocardial enhancer (Fig. 3B,B′).

From the observation that both *Igf2R* and *Igf2* are downregulated within the endocardial clusters, we wanted to determine whether endocardial proliferation was affected in *H2CKO* mutants. We conducted differential abundance analysis to determine cell type representation within *H2CKO* and control barcodes (Table S6; Fig. S8). Results indicated a significant increase in the number of barcodes in the endocardial population (cluster 7), as well as an increased number of barcodes in the cardiomyocyte population (clusters 0 and 1), which suggested that the loss of IGF2R might have affected the cell numbers in *H2CKO* mutants. The discovery of a HAND2-binding CNE −21 kb 5′ of the *Igf2r* TSS that drove endocardial-specific reporter expression supported this idea (Fig. 3A-B′). In order to determine the evolutionary conservation of this element, we used CLUSTWAL analysis, which indicated that conservation was limited within mammals (Fig. S9).

Two conserved non-coding elements drive expression of *Klf2* in ventricular endocardium

We next interrogated HAND2-occupied putative cardiac enhancers within the locus of the shear-stress master regulator KLF2. Expression analysis in both the scRNA-seq analysis and *in situ* hybridization (ISH) experiments revealed dynamic *Klf2* regulation within the heart (Fig. 2B,B′,D,D′). *Klf2* expression was specifically downregulated by HAND2 within the ventricular endocardium; however, *Klf2* endothelial expression was maintained within AV cushion endocardium (Fig. 2B′,D′). This observation was consistent with the downregulation of *Hand2* expression within the AV cushion endocardium post EMT, as previously reported (VanDusen et al., 2014a), and suggested that there was also HAND2-independent regulation of *Klf2* transcription within the AV cushion endocardium, as well as the systemic vasculature, in which *Hand2* is not expressed (VanDusen et al., 2014a).

Previously, a CNE located 100 bp upstream of the *Klf2* TSS had been shown to be responsive to shear stress (Huddleson et al., 2004),

Development (2023) 150, dev201341. doi:10.1242/dev.201341

Table 2. Summary of HAND2-occupied CNEs used for transgenesis test of enhancer activity

Element ID	Vista ID	Transgenic assay	Coordinates (mm10)	Size (bp)	Predicted target gene	Distance from TSS (kb)
Klf2-element (−16 kb)	mm2218	Hsp68-lacZ (random)	chr8:72302614-72304055	1442	*Klf2*	−16
Klf2-element (−50 kb)	mm2219	Hsp68-lacZ (random)	chr8:72266979-72269534	2556	*Klf2*	−50
Igf2-element	mm2220	H11 β-globin-lacZ	chr7:142586516-142587503	998	*Igf2*	+70
Igf2R element	mm2221	H11 β-globin-lacZ	chr17:12790150-12791705	1556	*Igf2r*	−21
Ptn-element	mm2222	H11 β-globin-lacZ	chr6:36784611-36785369	759	*Ptn*	+25
Tmem108-element	mm2223	H11 β-globin-lacZ	chr9:103758992-103759759	768	*Tmem108*	+2.5

but HAND2 DNA occupancy data did not indicate HAND2 DNA-binding within this element (Laurent et al., 2017). Interestingly, we identified two HAND2-occupied CNE within *Klf2*, one located −16 kb upstream of the *Klf2* TSS and another located −50 kb relative to the *Klf2* TSS (Fig. 3C-F′). The −16 kb *Klf2* CNE exhibited a high level of HAND2 occupancy and sequence conservation (Fig. 3C). Results showed that two out of eight F0 transgenics at E11.5 exhibited β-galactosidase staining within embryonic vasculature and endocardium (Fig. 3D,D′). Out of these two, we observed only one embryo that showed consistent staining throughout the left and right ventricular endocardium. The −50 kb *Klf2* CNE also exhibited robust HAND2 DNA occupancy and sequence conservation (Fig. 3E), and therefore was used to generate E11.5 F0 transgenics as well. Out of seven transgenics generated, four exhibited robust β-galactosidase staining within the endocardium and systemic vasculature (Fig. 3F,F′).

Given the higher consistency in endocardial/endothelial activity that we observed from the −50 kb *Klf2* enhancer element (57% of F0s), we generated stable *lacZ* transgenic lines using the −50 kb CNE (Fig. 4A). At E11.5, out of the 12 transgenic lines generated, five (41%) recapitulated consistent and robust β-galactosidase staining within the endocardium and systemic vasculature (Fig. S10). The remaining seven lines exhibited no observable β-galactosidase staining at E11.5. We next examined additional embryonic time points using a single line (line #901, Fig. S10). Analysis of reporter activity in E7.5 embryos revealed β-galactosidase staining within endothelial precursors, the blood islands (Fig. 4B), and within the dorsal aorta at E8.5 (Fig. 4C). At E9.5 and E10.5, the −50 kb CNE robustly drove β-galactosidase expression within endothelial structures, within the branchial arches and within intersomitic blood vessels (Fig. 4D,E arrow). Histological cross sections of β-galactosidase-stained torsos counterstained with nuclear fast red (NFR) at E10.5 revealed endocardial-specific staining at this time point (Fig. 4F-G′). Thus, we concluded that the −50 kb *Klf2* CNE functions as a transcriptional enhancer within the endothelial cells of the developing embryonic vasculature, endocardium and AV cushions (Fig. 4F′,G′).

Motif analysis of the −50 kb *Klf2* enhancer revealed the presence of three conserved Eboxes (Fig. 4H; Fig. S11) that lie within this established HAND2 DNA occupancy peak (Laurent et al., 2017). In order to determine whether HAND2 was able to interact with any of the three conserved Eboxes within this *Klf2* enhancer, we conducted ChIP assays in NIH-3T3 cells by co-transfecting plasmids encoding a 5′ Myc-tagged *Hand2* and an untagged *E12* (*Tcf3*) (Fig. 4H′). Negative controls used pCS2+myc samples immunoprecipitated with and without αMyc, and Myc-*Hand2* immunoprecipitated without αMyc. Using ChIP-PCR, we were able to observe HAND2 DNA binding at the 5′-most Ebox (Ebox1 CACCTG) within the *Klf2* enhancer in a dose-dependent manner (Fig. 4H′). The controls for this experiment employed primers recognizing the mouse *Rpl30* gene (Fig. 4H″). Taken together, the *in vitro* data supported HAND2 directly binding to and transcriptionally regulating *Klf2* through the −50 kb *Klf2* CNE.

HAND2 directly regulates expression of *Klf2* within the ventricular endocardium

To assess whether the endocardial −50 kb *Klf2* enhancer was dependent on HAND2 *in vivo*, we crossed the −50 kb *Klf2* enhancer *lacZ* transgenic reporter with the endocardial-specific *H2CKO*. E11.5 embryos were β-galactosidase stained, sectioned and counterstained with NFR (Fig. 4I). The −50 kb *Klf2* enhancer embryos (*lacZ*+ *Hand2*$^{fx/+}$) exhibited positive staining of trabecular endocardium (Fig. 4I,I′). In comparison, −50 kb *Klf2* enhancer *lacZ* reporter *H2CKO* embryos (*lacZ*+; *Nfatc1*^{cre} *Hand2*$^{fx/fx}$) showed a robust reduction in ventricular endocardial β-galactosidase staining (Fig. 4J,J′, arrows), whereas β-galactosidase staining within the endocardium over the developing AV cushions and systemic vasculature was maintained (Fig. 4J).

The −50 kb *Klf2* enhancer activity recapitulated the *Klf2* mRNA expression pattern throughout the embryo, with activity within the developing vasculature and the endocardium; however, crossing the −50 kb *Klf2* enhancer *lacZ* reporter to the *H2CKO* background only altered enhancer β-galactosidase staining within the ventricular endocardium and did not appreciably alter expression within the systemic vasculature or within the AV cushions. We found this result to be completely consistent with ISH analysis of *Klf2* expression in the *H2CKO* mutants (Fig. 2B′,D′). These data suggested to us that HAND2 DNA binding within this −50 kb *Klf2* endothelial/endocardial enhancer was necessary for its activity within the ventricular endocardium.

Deletion of the −50 kb *Klf2* endothelial/endocardial enhancer results in decreased *Klf2* ventricular endocardial expression

As the −50 kb *Klf2* endothelial/endocardial enhancer recapitulated *Klf2* vascular expression, we next tested its requirement for maintenance of *Klf2* expression via CRISPR-mediated genomic deletion in mice (Fig. S12A). Eleven enhancer-deleted lines were obtained and four of these were crossed for two generations with WT mice before they were intercrossed for homozygosity. *Klf2*$^{\Delta\text{-}50:(3.9kb)/\Delta\text{-}50:(3.9kb)}$ mice were viable and were born at Mendelian frequencies in four outcrossed founder lines (Fig. S12B). A single line was then set up for timed pregnancies and E11.5 embryos were evaluated for *Klf2* expression (Fig. 5A,B). *Klf2* expression was visibly lower within the endocardium. In contrast, *Hand2* expression within adjacent sections appeared to be unchanged between controls and *Klf2*$^{\Delta\text{-}50:(3.9kb)/\Delta\text{-}50:(3.9kb)}$ hearts (Fig. 5C,D). We performed qRT-PCR on E11.5 ventricles to confirm that the observed *Klf2* expression drop in the *Klf2*$^{\Delta\text{-}50:(3.9kb)/\Delta\text{-}50:(3.9kb)}$ homozygous hearts was significant. We isolated eight *Klf2*$^{\Delta\text{-}50:(3.9kb)/\Delta\text{-}50:(3.9kb)}$ and ten WT ventricles for qRT-PCR (Fig. 5E). As predicted by the ISH

Development (2023) 150, dev201341. doi:10.1242/dev.201341

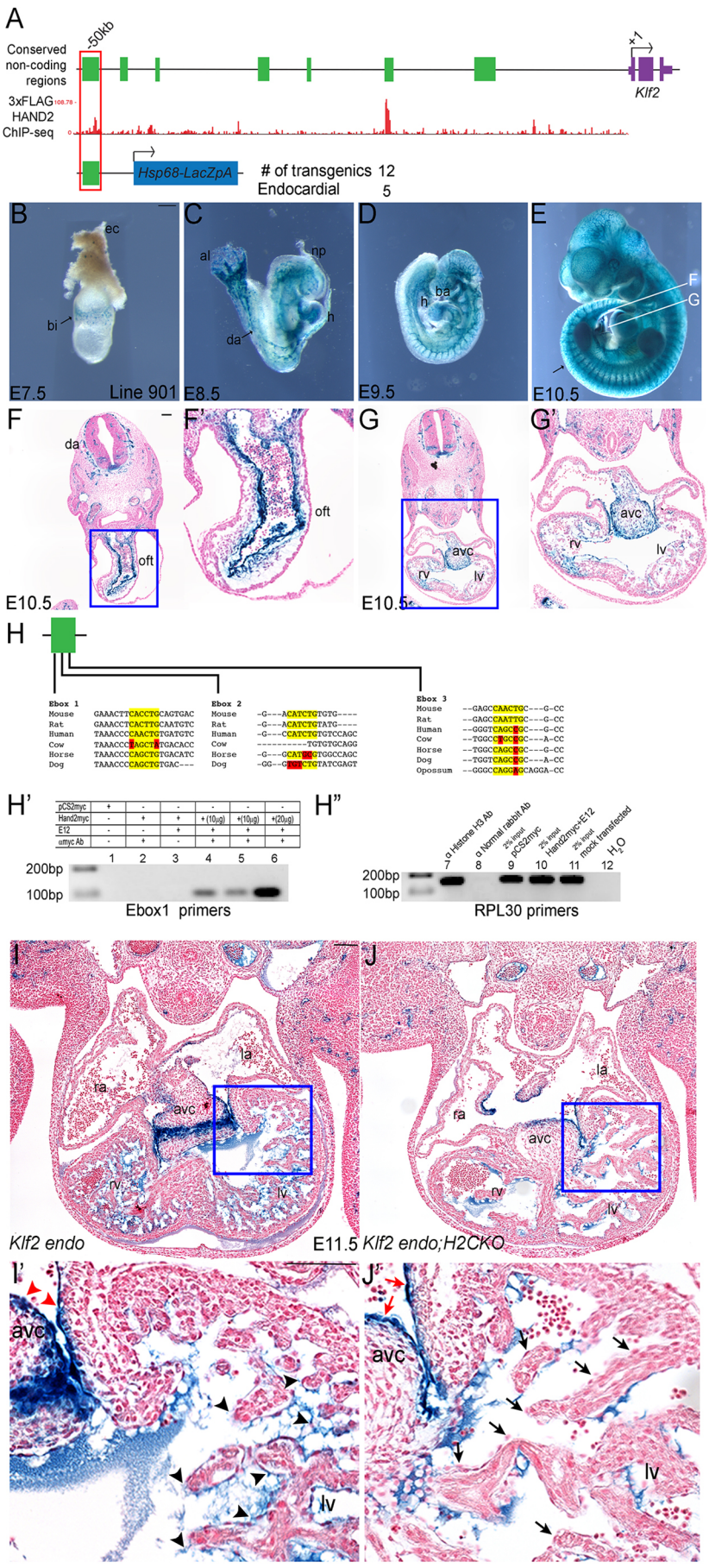

Fig. 4. HAND2 responsive conserved *Klf2* enhancer is HAND2 dependent. (A) Conserved non-coding regions (green boxes) upstream of *Klf2* TSS (+1). *HAND2*^{3xFlag} ChIP-seq data (Laurent et al., 2017) showing regions of *Hand2* binding. (B-E) The −50 kb HAND2-binding conserved non-coding *Klf2* region used to make stable transgenics, number of stable transgenic lines obtained and number of lines showing endocardial staining of transgene. β-galactosidase staining of E7.5, E8.5, E9.5, E10.5 embryos from founder line 901. Plane of cross section for outflow tract (oft) and four chamber view in F and G are indicated by white lines in E. Arrow in E indicates intersomitic blood vessels. (F,F′) Transverse sections counterstained with NFR showing β-galactosidase staining in the outflow tract. Blue box in F indicates area magnified in F′. (G,G′) Transverse sections counterstained with NFR showing β-galactosidase staining in four chamber view. Blue box in G indicates area magnified in G′. (H) Conserved Eboxes in −50 kb *Klf2* enhancer. Yellow base pairs indicate regions of conservation. Red base pairs indicate regions of non-conservation within the canonical Ebox sequence. (H′) ChIP experiment in NIH 3T3s transfected with plasmids as indicated. Primers specific for Ebox1 showed binding when *mycHand2* construct is co-transfected with *E12* in a dose-dependent manner. Lane 1, pCS2myc empty vector; lane 2, pCSmyc; anti-myc antibody; lane 3, *mycHand2*, no antibody; lane 4, 10 µg *mycHand2+E12*; anti-myc antibody; lane 5, 10 µg *mycHand2+E12*; anti-myc antibody; lane 6, 20 µg *Hand2+E12*; anti-myc antibody. (H″) Control primers against mouse RPL30 used to show control ChIP using anti-HistoneH3 antibody and 2% input samples as indicated. Negative control using ChIP with anti-normal rabbit antibody does not show signal. Primers used for PCR specific for mouse RPL30 gene intron 2. Lane 7, anti-Histone H3 antibody, positive control; lane 8, anti-normal rabbit antibody; negative control; lane 9, 2% input, pCS2myc; anti-Histone H3 antibody; lane 10, 2% input, *mycHand2+E12*; anti-Histone H3 antibody; lane 11, 2% input, mock transfected, anti-Histone H3 antibody; lane 12, H_2O. (I,I′) The −50 kb *Klf2* enhancer at E11.5 was stained for X-gal, sectioned and counterstained with NFR. Blue box in I indicates area magnified in I′. Black arrowheads indicate ventricular endocardium with X-gal staining. Red arrowheads indicate X-gal staining within the endocardium covering the AV cushion. (J,J′) *Nfatc1*^{Cre} *Hand2*$^{fx/fx}$ with *Klf2* enhancer transgene at E11.5. Blue box in J indicates area magnified in J′. Black arrows indicate loss of enhancer activity within the ventricular endocardium. Red arrows indicate X-gal staining within the endocardium covering the AV cushion. Scale bars: 200 µm (B); 100 µm (F,I). al, allantois; avc, atrioventricular cushion; ba, branchial arches; bi, blood islands; da, dorsal aorta; ec, ectoplacental cone; h, heart; la, left atrium; lv, left ventricle; np, neural plexus; ra, right atrium; rv, right ventricle.

Development (2023) 150, dev201341. doi:10.1242/dev.201341

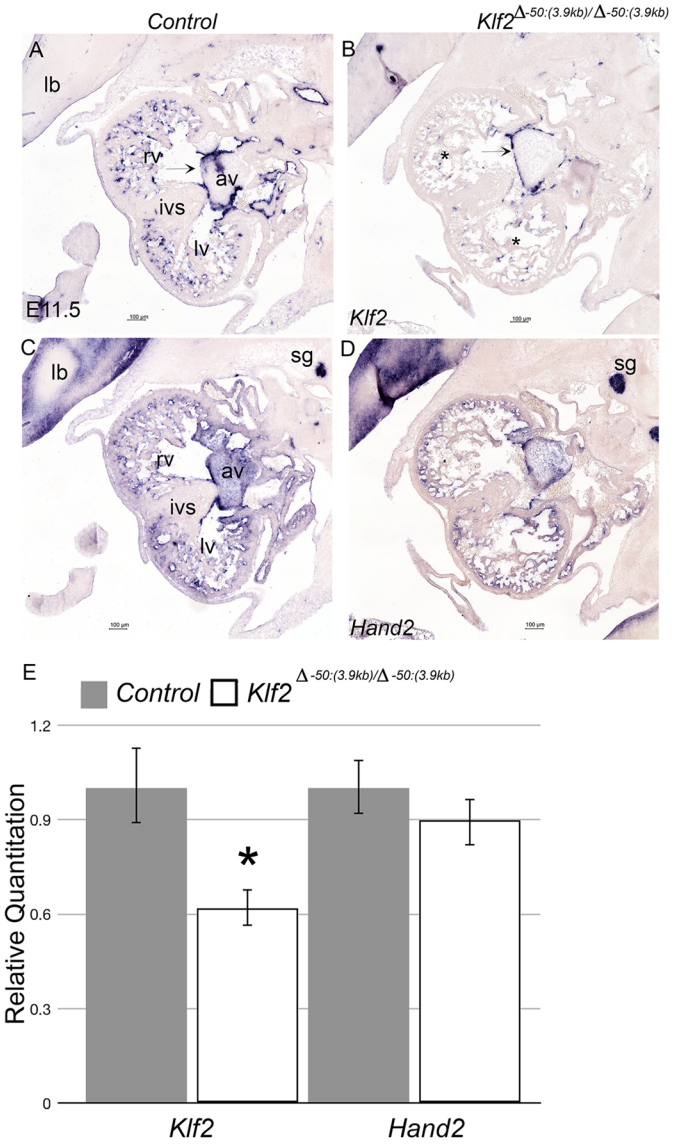

Fig. 5. CRISPR/Cas9 mediated deletion of −50 kb *Klf2* enhancer results in reduced *Klf2* ventricular endocardial expression. (A,C) Representative *in-situ* hybridization section showing *Hand2* and *Klf2* expression in control E11.5 embryos. (B,D) Representative *in-situ* hybridization section showing *Hand2* and *Klf2* expression in $Klf2^{\Delta\text{-}50kb(3.9kb)/\Delta\text{-}50kb(3.9kb)}$ E11.5 embryos. Arrow indicates maintained expression within the endocardium overlying the AV cushions. Asterisks in B mark loss of gene expression within the ventricles of $Klf2^{\Delta\text{-}50kb(3.9kb)/\Delta\text{-}50kb(3.9kb)}$ embryos. av, atrioventricular cushion; ivs, interventricular septum; lb, limb bud; lv, left ventricle; rv, right ventricle; sg, sympathetic ganglia. (E) qRT-PCR analysis from E11.5 ventricle cDNA [8 control and 10 $Klf2^{\Delta\text{-}50kb(3.9kb)/\Delta\text{-}50kb(3.9kb)}$] showing significant downregulation of *Klf2* expression within $Klf2^{\Delta\text{-}50kb(3.9kb)/\Delta\text{-}50kb(3.9kb)}$ ventricles when compared with controls (*P-value=0.01). *Hand2* expression is not significantly altered.

analysis, *Klf2* expression levels were significantly lower (P<0.001) in $Klf2^{\Delta\text{-}50:(3.9kb)/\Delta\text{-}50:(3.9kb}$ ventricles compared with control ventricles, ∼60% of what is observed in WT (Fig. 5E). Results showed that *Hand2* expression was unchanged within $Klf2^{\Delta\text{-}50:(3.9kb)/\Delta\text{-}50:(3.9kb)}$ hearts compared with WT controls (Fig. 5E). Given that the −50 kb enhancer recapitulated all *Klf2* embryonic expression but was only affected by HAND2 within the ventricular endocardium, the observed 40% decrease in endocardial expression was in line with our observations.

DISCUSSION

Loss of *Hand2* within the endocardium disrupts NOTCH signaling resulting in a hypotrabeculated single ventricle composed of hypervascularized free walls (VanDusen et al., 2014a). To gain a better understanding on the gene regulatory networks in which HAND2 facilitates ventricular morphogenesis downstream of NOTCH1, we used scRNA-seq at E11.5, combined with established HAND2 DNA occupancy data (Laurent et al., 2017) to interrogate the role of HAND2 in regulating the endocardial gene regulatory networks. IPA analysis revealed a number of pathways known to be required for heart development that showed misregulation within the identified endothelial/endocardial cell populations (Fig. 1). These analyses revealed disruption in several pathways such as wound healing, pulmonary fibrosis and healing, tumor microenvironment (including HIF1α signaling) as well as the Apelin pathway, which includes shear-stress response regulation and is the pathway most relevant to endocardial roles in cardiogenesis (Table 1; Fig. S5; Table S2). Collectively, these pathways play roles in the endocardial response to vascularization of the myocardium, organ growth and communication with the underlying myocardium coordinating septation and trabeculation. A number of significantly regulated genes, for example *Fn1*, *Ece1* and *Edn1*, exhibit altered expression, but do not exhibit robust HAND2 DNA occupancy in *cis* (Laurent et al., 2017). Although such genes are influenced by HAND2 function, they are likely not transcriptionally regulated by HAND2 directly; nevertheless, their altered expression fits with HAND2 function in previous studies. In epicardial *Hand2* deletion, although *Fn1* expression is unaltered when comparing control with mutants, FN1 organization is altered within *H2CKO* epicardial cells (Barnes et al., 2011). During jaw morphogenesis, *Hand2* has been established as lying downstream of EDN1 signaling and plays an important negative feedback role once activated, by repressing *Dlx5* and *Dlx6* expression within the ventral-most portion of the mandible mesoderm (Barron et al., 2011; Charité et al., 2001; Clouthier et al., 2000; Vincentz et al., 2016).

We chose five target genes – *Igf2*, *Igf2R*, *Ptn*, *Tmem108* and *Klf2* – to investigate further for putative endocardial/endothelial HAND2-dependent enhancers (Fig. 3; Fig. S7), based on our comparisons of highly misregulated genes with robust HAND2 DNA occupancy data to locate potential *cis*-regulatory elements (Laurent et al., 2017). CNE peaks bound by HAND2 from *Igf2*, *Tmem108* and *Ptn* did not reveal any transcriptional activity (Fig. S7). More interestingly, we discovered three endocardial/endothelial enhancers that did have transcriptional activity, one CNE 5′ of the *Igf2R* TSS, and two CNE upstream of the *Klf2* TSS (Fig. 3).

The crucial source of IGF2 in the heart is from the epicardium (Shen et al., 2015). Epicardial IGF2 diffuses into the heart where it can bind to its receptors, including IGF2R. Binding to IGF2R facilitates IGF2 degradation within the lysosomes (Harris and Westwood, 2012). Knockout of IGF2R within endothelial cells using *Tie2Cre* does not result in embryonic lethality; however, cardiac-specific phenotypes have not been examined (Sandovici et al., 2022). Our data suggest that IGF2R plays a role within cardiac endothelium in a HAND2-dependent manner. We observed a significant change in cell numbers within *H2CKO* mutants and controls (Table S5), although it is yet to be determined whether increased proliferation is the cause. Cell proliferation within E10.5 right ventricle of *Tie2Cre*-mediated *H2CKO* hearts did not show a significant difference in cell numbers (VanDusen et al., 2014a,b).

As KLF2 is a known master regulator of shear-stress response and is a significant regulator within the Apelin regulatory network, we

Development (2023) 150, dev201341. doi:10.1242/dev.201341

engineered a stable *Klf2* reporter line using the more robustly consistent endothelial/endocardial CNE located at −50 kb of the *Klf2* TSS. Reporter expression analysis reveals that this *Klf2* CNE recapitulates all the *Klf2* endothelial/endocardial expression and is dependent on HAND2 only within the endocardium, correlating directly with our *Klf2* mRNA expression regulation data (Figs 2 and 4). KLF2 is expressed in regions of endothelium exposed to high shear stress (Goddard et al., 2017). In the developing heart such high shear-stress regions include the endocardium overlying the developing valves and the developing ventricular trabeculae, with *Klf2* expression levels varying within regions of differential shear force (Goddard et al., 2017). Loss of HAND2 does not appear to impact *Klf2* expression within the regions of endocardium overlying the developing valve cushions where *Hand2* expression is already downregulated (VanDusen et al., 2014a,b). Previous work characterizing conserved non-coding elements at the *Klf2* genomic locus identified a 60 bp enhancer element located 100 bp upstream of *Klf2* TSS that is responsive to shear stress within mouse endothelial cells in culture (Huddleson et al., 2004). It is currently unclear whether either the −16 or −50 kb CNE enhancers are shear-stress responsive, but it is clear that the −50 kb enhancer can recapitulate all *Klf2* mRNA expression domains during embryogenesis and the majority of its activity is HAND2-independent, given that HAND2 is not expressed within the systemic vasculature (Fig. 4). As one would expect, the −50 kb *Klf2* enhancer element contains other consensus binding sequences including the myocyte enhancer factor 2 (MEF2) family of transcription factors that are established regulators for vascular homeostasis and are transcriptional activators of *Klf2* (De Val and Black, 2009; Lu et al., 2021). Analysis of DNA occupancy data shows that both the −16 kb and −50 kb *Klf2* enhancers have conserved MEF2C binding (Akerberg et al., 2019). Given the established role of MEF2C in endothelial integrity and homeostasis, it is not surprising that the loss of *Hand2* does not lead to loss of vascular KLF2 expression.

Lineage tracing analysis shows that the endocardium is a primary source of cells that eventually gives rise to coronary vessels (Sharma et al., 2017). Studies in mouse models demonstrate that both endocardial and epicardial cells migrate into the myocardium to give rise to patent vessels (Sharma et al., 2017) and that these coronaries form within different zones of the myocardium (septum versus free walls of the ventricles) (Chen et al., 2014). This suggests that coronary angiogenesis is driven by distinct mechanisms within different regions of the developing heart. The cellular origin of coronary vasculature is a source of some debate, the current consensus being that coronaries of the ventricular free wall are derived from the epicardium and the sinus venosus, whereas interventricular septal coronaries are derived from the ventricular endocardium (Phansalkar et al., 2021; Rhee et al., 2021; Zhang et al., 2016).

Klf2 undergoes a robust shear-stress response, as at least 50% of the highly regulated flow genes are dependent on the upregulation of *Klf2* (Parmar et al., 2006). *Klf2* expression within the endocardial cells of the ventricular wall fated to contribute to coronaries in these endocardial cells is HAND2 dependent. Indeed, one of the most striking observations in *H2CKO* heart endocardium and vasculature is the persistent expression of *Lyve1* beyond its normal endocardial downregulation by E13.5 (VanDusen et al., 2014a). LYVE1-expressing endocardium ultimately contributes to peripheral cardiac macrophages and the developing lymphatic vasculature of the heart, in which vessel pressures are far less than those encountered in blood vasculature (Pinto et al., 2012). It is an appealing idea that a defective shear-stress response of the ventricular endocardium could result in improper development and/or maturation of the ventricular endocardium into the correct sub-fates that result in hypervascularization of the ventricular walls composed of an immature, more lymphatic-like, endothelium. Further support for this idea comes from multiple lines of evidence demonstrating that KLF2 inhibits angiogenesis by interacting with the *Kdr* promoter (Bhattacharya et al., 2005), as the loss of KLF2 also leads to hypervascularization (Kawanami et al., 2009). In our *H2CKO* data, we observed a modest increase in *Kdr* expression in cluster 7 (log2FC 0.13, not significant) which could be supportive of this possible mechanism.

Multiple genetic knockouts have been generated to study KLF2 function within endothelial cells. The *Klf2* systemic knockout is embryonically lethal between E12.5 to E14.5 due to severe intra-embryonic and intra-amniotic hemorrhaging (Kuo et al., 1997; Wani et al., 1998). Endothelial knockout of *Klf2* (and the related *Klf4*) using tamoxifen-inducible *Cdh5-Ert2Cre* in 8- to 10-week-old adult mice causes vascular leakage leading to hemorrhaging and death (Sangwung et al., 2017). Embryonic endothelial knockout of *Klf2* using *Tie2Cre* exhibits increased systolic stroke volumes and high output heart failure leading to death at E14.5 due to abnormal vessel tone (Lee et al., 2006) and endocardial knockout of *Klf2* using $Nfatc1^{Cre}$ results in embryonic lethality by E14.5 due to septal defects arising from the failure of cushion remodeling (Goddard et al., 2017). Moreover, work in zebrafish demonstrates that flow-responsive *Klf2* activates notch signaling, through a mechanism that employs endocardial primary cilia (Li et al., 2020).

Given that $Klf2^{\Delta\text{-}50:(3.9kb)/\Delta\text{-}50:(3.9kb)}$ mice exhibit only a 40% reduction in *Klf2* endocardial expression and appear to maintain systemic vascular expression through other identified enhancers (Fig. 5), it is not surprising that the removal of this −50 kb *Klf2* CNE does not result in embryonic lethality and that mice are viable and fertile. What we do not know currently is the *Klf2* expression threshold that results in the observed embryonic vascular phenotypes or whether any KLF2 endocardial-specific phenotypes contribute to the observed embryonic lethality. Collectively, these data demonstrate that HAND2 integrates endocardial transcriptional networks reaching beyond the NOTCH pathway and including shear-stress response, thereby revealing a number of important roles during endocardial morphogenesis.

MATERIALS AND METHODS

Mouse strains and genotyping

$Hand2^{fx/fx}$ mice (Morikawa and Cserjesi, 2008; The Jackson Laboratory, strain 027727) and $Nfatc1^{cre}$ (Wu et al., 2012) were genotyped as described previously (VanDusen et al., 2014a). The University of Michigan Transgenic Animal Model Core generated *lacZ* transgenic enhancer lines in the FVB background. Twelve transmitting founder lines were screened for X-gal staining and enhancer activity. Transgenic founders and embryos were genotyped using primers spanning the enhancer and *HSP68* promoter 5′-AGCCTGTGAGAGAGACCCAT-3′ and 5′-GATGTTCCTGGAGCT-CGGTA-3′. Genotyping for other alleles was carried out using Southern blots as previously described (George and Firulli, 2021). All animal maintenance and procedures were performed in accordance with the Indiana University School of Medicine protocol 20090, and University of Michigan School of Medicine. Animal work at Lawrence Berkeley National Laboratory (LBNL) was reviewed and approved by the LBNL Animal Welfare Committee.

Single cell RNA-seq

E11.5 embryos were dissected in cold PBS and placed in PBS with 1% fetal bovine serum (FBS) solution on ice until dissociation (~3 h). Yolk-sac DNA was extracted (QuickExtract DNA Extraction Solution, Epicentre) and

Development (2023) 150, dev201341. doi:10.1242/dev.201341

used for genotyping to distinguish heterozygous and homozygous *Hand2* conditional alleles. The *Rosa*^{mTmG} allele fluorescence was used to determine *Nfatc1*^{cre} status. Dissected cardiac tissue was incubated in 750 µl TrypLE (Thermo Fisher Scientific) for 5 min at 37°C, triturated with a 200-µl wide-bore pipette tip. The cell suspension was quenched with 750 µl DMEM with 10% FBS. Cells were filtered through a 30-µm cell strainer (MACS SmartStrainer), centrifuged at 300 ***g*** for 5 min, and washed once with 750 µl PBS with 0.5% bovine serum albumin (BSA). Cells were resuspended in 30 µl PBS with 0.5% BSA (10x Genomics). Single-cell droplet libraries from this suspension were generated using the Chromium NextGEM Single Cell 3′ Reagent Kits User Guide, CG000204 Rev D (10x Genomics), according to the manufacturer's instructions. Briefly, each clean single cell suspension was counted with hemocytometer under a microscope for cell number and cell viability. Only single cell suspensions with a viability of >90% and minimal cell debris and aggregation were used for further processing. The resulting library was sequenced in a custom program for 28b plus 91b paired-end sequencing on Illumina NovaSeq 6000. About 50,000 reads per cell were generated and 91% of the sequencing reads reached Q30 (99.9% base call accuracy).

Sequenced reads were aligned to a mouse transcriptome reference built from GRCm38.p6 (Genome Reference Consortium Mouse Build 38 patch release 6) combined with eGFP and dTomato gene sequences using the software 10x Genomics Cell Ranger 5.0.1 (Zheng et al., 2017). Reads from the cells associated with more than 1000 unique molecular identifiers from hemoglobin-related genes (*Hbb-bt*, *Hbb-bs*, *Hbb-bh2*, *Hbb-bh1*, *Hbb-y*, *Hba-x*, *Hba-a1*, *Hbq1b*, *Hba-a2* and *Hbq1a*) were excluded from further analysis. The downstream data exploration and differential gene expression analysis was conducted using the R package, Seurat V4 (Hao et al., 2021). As per the standard pre-processing workflow for scRNA-seq data in Seurat, cells with more than 2500 unique features were filtered out. The feature expression values for each cell were normalized using the standard 'LogNormalize' method with default parameter values. The Seurat objects derived from control (WT) and *H2CKO* mutant data were integrated using the anchors found using canonical correlation analysis (CCA) with the neighbor search space specified using 1 to 20 dimensions [FindIntegrationAnchors(reduction="cca", dims=1:20)]. The integrated dataset was subjected to linear transformation followed by linear dimensionality reduction using principal component analysis (PCA). Clusters were identified from the shared nearest neighbor graph [FindNeighbors(reduction="pca", dims=1:20)] with the resolution set to 0.5 [FindClusters(resolution=0.5)] and were visualized using the UMAP non-linear dimensional reduction technique. For each cluster, the differentially expressed genes between control and *H2CKO* genotypes were called using a Wilcoxon Rank Sum test [FindMarkers(test.use="wilcox")]. Genes with Bonferroni corrected *P*-values not more than 0.05 were considered significantly differentially expressed. For IPA analysis, the pathways relevant to the significantly differentially expressed genes (FDR≤0.05) were identified using the Core Analysis of the IPA software (Qiagen, https://www.qiagenbio-informatics.com/products/ingenuity-pathway-analysis).

CRISPR/Cas9 mediated deletion of −50 kb *Klf2* enhancer

To generate the CRISPR-KO, single guide RNAs flanking the −50 kb *Klf2* enhancer were designed by University of Michigan Transgenic Core (5′-CTACTACTTGGCAGGTTGGAGGG-3′ and 5′-GTCAAAGGGACC-TGGTAGTTTGG-3′). Guide RNAs were tested for inducing chromosome breaks before microinjection. We screened 114 potential founders with PCR primers spanning the deletion (5′-ATGTGTGTGCATCTGGGGAGCA-GAG-3′ and 5′-CCAGAGTGACTTTTCAGGCACAGGGG-3′) which generated a 450 bp product for the deleted allele. Primers within the deleted region were used to confirm a true indel (WT 5′-CTTATAACCTC-CATTTCCTCCTCTGGG-′3 and WT 3′-CTTCGTGGTTTCCTGCT-TGCTAAGATG-′3) that generates a 350 bp product for the WT allele. PCR products from 31 positive founders were cloned and sequence verified to characterize the deletion. A probe for Southern blot was designed using the following primers to clone out a 332 bp fragment from murine genomic DNA: 5′-CAAGGCCTTCCAGTACCAGG-3′ and 5′-TCTCAGT-GGAGCTTGCTGTG-3′. The probe detects an RFLP in EcoRV-digested genomic DNA, 9.5 kb in WT allele and 5.6 kb in the CRISPR deleted allele [*Klf2* $^{\Delta\text{-}50kb(3.9kb)}$]. Selected founders were outcrossed for two generations before being bred to homozygosity.

Transgenic mouse reporter assays

Mouse transgenesis at LBNL was performed in *Mus musculus* FVB strain mice. Animals of both sexes were used in these analyses and mouse embryos were excluded from further analysis if they did not encode the reporter transgene or if the developmental stage was not correct. For validation of *in vivo* enhancer activities, random *Hsp68-lacZ* transgenesis (for *Klf2* elements) and enSERT was used for site-directed insertion of transgenic constructs at the *H11* safe-harbor locus (Osterwalder et al., 2022; Kvon et al., 2020). EnSERT is based on pronuclear co-injection of *Cas9*, sgRNAs and a H11-homology arms-containing targeting vector encoding a candidate enhancer element upstream of a minimal promoter and a reporter protein (Kvon et al., 2020; Osterwalder et al., 2022). Related genomic enhancer coordinates are listed in Table 2. Predicted enhancer regions were PCR-amplified from mouse genomic DNA from WT FVB mice and cloned into a modified targeting vector encoding either an *Hsp68-lacZ* cassette (for random integration) or a human β-globin (*HBB*) minimal promoter upstream of a *lacZ* reporter (for enSERT). Embryos were excluded from further analysis if they did not contain a reporter transgene. CD-1 females served as pseudo-pregnant recipients for embryo transfer to produce transgenic embryos which were collected at E11.5 and stained with X-gal using standard techniques (Osterwalder et al., 2022). Embryos were harvested from timed matings at the timepoints indicated and pre-fixed in 2% paraformaldehyde-0.2% glutaraldehyde and stained as previously described (VanDusen et al., 2014a; Vincentz et al., 2019). After overnight staining at room temperature, embryos were post-fixed in 4% paraformaldehyde before imaging and sectioning. The number of tandems over total transgenics confirmed the negative activity of these elements as obtaining *n*=2 tandems (PCR-determined multicopy insertions at *H11*) for enSERT is sufficient to conclude whether an element is active or inactive (Kvon et al., 2020; Osterwalder et al., 2022).

Histology

If stained, β-galactosidase-stained embryos were post-fixed, washed in PBS, dehydrated, embedded, sectioned and NFR stained as previously described (George and Firulli, 2021; Vincentz et al., 2019). Images were acquired on the Keyence BZ-X800 florescence microscope system or the Leica DM5000 B compound microscope.

Cloning

Conserved non-coding putative HAND2 binding regions were cloned out from genomic mouse DNA using the following primers: *Igf2* 5′-GAGAAGCTGGCAGATCAGGCTGTG-3′ and 5′-TGCTTCTGTTG-AGAGGAGACAGTCTGG-3′; *Igf2r* 5′-TTGCCTGCATGTAAGTGTG-CCTGG-3′ and 5′-TGTCTCTCAGGCTTCCTGTCTGGC-3′; *Ptn* 5′-ATTTCAGCTGGACTGCCATGGCAG-3′ and 5′-GGCTGGAAGAG-GAGGCAAACAGAG-3′; *Tmem108* 5′-CATCATCACCATCACCATC-GTCGTCG-3′ and 5′-GTATGCAGTGGACCTCTTTGACTTGTCAG-3′; *Klf2* enhancer −16 kb element 5′-ATCTGTCCACCTCTACCTTCCA-3′ and 5′-AGTGGCTCTGACAACCTGAGAT-3′; *Klf2* enhancer −50 kb element 5′-TGAACCTCCATTGATACACACC-3′ and 5′-GTCCCTAAG-GATCATGTTGAGC-3′. Amplified sequences were Gibson (New England Biolabs) cloned into the *pCR4-bG::lacZ-H11* enSERT vector and used to generate F0 enhancer transgenics. Briefly, the enSERT system uses CRISPR/Cas9-mediated site directed transgenesis at the murine *H11* locus resulting in genomic integration of the human β-globin promoter with the enhancer element to be tested and the *lacZ* reporter cassette (Kvon et al., 2020). F0 embryos were harvested at E11.5 for β-galactosidase staining and analysis.

To generate the −50 kb *Klf2* stable transgenic allele, primers corresponding to genomic region chr8:74791237-74793083 (mm9) (5′-AAGGGCCA-GATGTGCTGAAA-3′ and 5′-GGCTGGTCTCGAACTCACAA-3′) were cloned into the *HSP68-lacZ* vector backbone as described previously (Vincentz et al., 2019) and used to create stable β-galactosidase-expressing mouse transgenic lines.

Development (2023) 150, dev201341. doi:10.1242/dev.201341

In-situ hybridization

Section ISH was performed on 10 µm paraffin sections as described previously (George and Firulli, 2021). Whole mount ISH was performed using E10.5 embryos as described previously (George and Firulli, 2021). Antisense digoxygenin-labeled riboprobes were synthesized using T7, T3 or SP6 polymerases (Promega) and DIG-Labeling Mix (Roche) using the following plasmid templates: *Hand2*, *Klf2*.

Quantitative real time PCR

Total RNA was isolated from E11.5 ventricles using the High Pure RNA Isolation Kit (Roche). RNA was used to synthesize cDNA using the High-Capacity cDNA Reverse Transcription Kit (Applied Biosystems). For qRT-PCR, cDNA was amplified using TaqMan Probe-Based Gene Expression Assays (Applied Biosystems) to quantify gene expression. qRT-PCR reactions were run on the QuantStudio 3 Real-Time PCR System (Thermo Fisher Scientific). Normalization to glyceraldehyde 3-phosphate dehydrogenase (*GAPDH*) was used to determine relative gene expression and statistical analysis was automatically applied by the instrument software. Significance of qRT-PCR results were determined by an unpaired two-tailed Student's *t*-test followed by post hoc Benjamini–Hochberg FDR correction as automatically calculated by the QuantStudio3 qRT-PCR thermal cycler software analysis package. Data are presented as relative quantitation values, where error bars depict the maximum and minimum values of each series of samples. A minimum *n* of 8 is used in all assays.

ChIP PCR assays

For ChIP assays, NIH3T3 cells were transfected with Lipofectamine 3000 with plus reagent (Invitrogen) according to the manufacturer's instructions with pCS2+Myc-Hand2, pCS2+Myc-E12 or pCS2 control constructs as indicated. After culturing for 48 h, SimpleChIP plus enzymatic chromatin IP kit (Cell Signaling Technology) was used as per the manufacturer's recommendations, and PCR was used to detect ChIP products run out on agarose gel.

Acknowledgements

We thank Danny Carney and Chloe Ferguson for technical assistance. The *Klf2* expression vector used to generate the ISH probe was a kind gift from Jonathan A. Epstein. We thank Fabrice Darbellay for the generation of the β-globin-*lacZ* H11-targeting vector backbone and Nathan VanDusen for helpful comments.

Competing interests

The authors declare no competing or financial interests.

Author contributions

Conceptualization: A.B.F.; Methodology: R.M.G., B.A.F., A.B.F.; Validation: R.M.G., R.P., D.B.R., B.J.M.; Formal analysis: B.A.F., D.B.R.; Investigation: R.M.G., B.A.F., R.P., L.A.P., M.O., A.B.F.; Resources: L.A.P., A.B.F.; Data curation: R.M.G., B.A.F., B.J.M.; Writing - original draft: R.M.G.; Writing - review & editing: R.M.G., B.A.F., M.O., A.B.F.; Visualization: R.P., D.B.R.; Supervision: D.B.R., L.A.P., A.B.F.; Project administration: A.B.F.; Funding acquisition: A.B.F.

Funding

This work is supported by the National Institutes of Health (1R01DE02909, 1R01 HL145060, 2P01HL134599 and 1R01HL120920-01). M.O. was supported by Schweizerischer Nationalfonds zur Förderung der Wissenschaftlichen Forschung grant PCEFP3_186993. L.A.P. and the research conducted at the E.O. Lawrence Berkeley National Laboratory was supported by a National Institutes of Health grant R01HG003988 (to L.A.P.) and performed under Department of Energy Contract DE-AC02-05CH11231, University of California. Infrastructural support at the Herman B Wells Center for Pediatric Research is in part supported by the generosity of the Riley Children's Foundation, Division of Pediatric Cardiology and the Carrolton Buehl McCulloch Chair of Pediatrics. Deposited in PMC for release after 12 months.

Data availability

Sequence data have been deposited in GEO under accession number GSE210221.

People behind the papers

This article has an associated People behind the papers interview with some of the authors.

References

Akerberg, B. N., Gu, F., VanDusen, N. J., Zhang, X., Dong, R., Li, K., Zhang, B., Zhou, B., Sethi, I., Ma, Q. et al. (2019). A reference map of murine cardiac transcription factor chromatin occupancy identifies dynamic and conserved enhancers. *Nat. Commun.* **10**, 4907. doi:10.1038/s41467-019-12812-3

Barnes, R. M., Firulli, B. A., VanDusen, N. J., Morikawa, Y., Conway, S. J., Cserjesi, P., Vincentz, J. W. and Firulli, A. B. (2011). Hand2 loss-of-function in Hand1-expressing cells reveals distinct roles in epicardial and coronary vessel development. *Circ. Res.* **108**, 940-949. doi:10.1161/CIRCRESAHA.110.233171

Barron, F., Woods, C., Kuhn, K., Bishop, J., Howard, M. J. and Clouthier, D. E. (2011). Downregulation of Dlx5 and Dlx6 expression by Hand2 is essential for initiation of tongue morphogenesis. *Development* **138**, 2249-2259. doi:10.1242/dev.056929

Bhattacharya, R., Senbanerjee, S., Lin, Z., Mir, S., Hamik, A., Wang, P., Mukherjee, P., Mukhopadhyay, D. and Jain, M. K. (2005). Inhibition of vascular permeability factor/vascular endothelial growth factor-mediated angiogenesis by the Kruppel-like factor KLF2. *J. Biol. Chem.* **280**, 28848-28851. doi:10.1074/jbc.C500200200

Bochmann, L., Sarathchandra, P., Mori, F., Lara-Pezzi, E., Lazzaro, D. and Rosenthal, N. (2010). Revealing new mouse epicardial cell markers through transcriptomics. *PLoS ONE* **5**, e11429. doi:10.1371/journal.pone.0011429

Braulke, T. (1999). Type-2 IGF receptor: a multi-ligand binding protein. *Horm. Metab. Res.* **31**, 242-246. doi:10.1055/s-2007-978725

Charité, J., McFadden, D. G., Merlo, G., Levi, G., Clouthier, D. E., Yanagisawa, M., Richardson, J. A. and Olson, E. N. (2001). Role of Dlx6 in regulation of an endothelin-1-dependent, dHAND branchial arch enhancer. *Genes Dev.* **15**, 3039-3049. doi:10.1101/gad.931701

Chen, H., Shi, S., Acosta, L., Li, W., Lu, J., Bao, S., Chen, Z., Yang, Z., Schneider, M. D., Chien, K. R. et al. (2004). BMP10 is essential for maintaining cardiac growth during murine cardiogenesis. *Development* **131**, 2219-2231. doi:10.1242/dev.01094

Chen, H. I., Sharma, B., Akerberg, B. N., Numi, H. J., Kivelä, R., Saharinen, P., Aghajanian, H., McKay, A. S., Bogard, P. E., Chang, A. H. et al. (2014). The sinus venosus contributes to coronary vasculature through VEGFC-stimulated angiogenesis. *Development* **141**, 4500-4512. doi:10.1242/dev.113639

Chiplunkar, A. R., Lung, T. K., Alhashem, Y., Koppenhaver, B. A., Salloum, F. N., Kukreja, R. C., Haar, J. L. and Lloyd, J. A. (2013). Krüppel-like factor 2 is required for normal mouse cardiac development. *PLoS ONE* **8**, e54891. doi:10.1371/journal.pone.0054891

Clouthier, D. E., Williams, S. C., Yanagisawa, H., Wieduwilt, M., Richardson, J. A. and Yanagisawa, M. (2000). Signaling pathways crucial for craniofacial development revealed by endothelin-A receptor-deficient mice. *Dev. Biol.* **217**, 10-24. doi:10.1006/dbio.1999.9527

De Val, S. and Black, B. L. (2009). Transcriptional control of endothelial cell development. *Dev. Cell* **16**, 180-195. doi:10.1016/j.devcel.2009.01.014

Del Monte-Nieto, G., Ramialison, M., Adam, A. A. S., Wu, B., Aharonov, A., D'Uva, G., Bourke, L. M., Pitulescu, M. E., Chen, H., de la Pompa, J. L. et al. (2018). Control of cardiac jelly dynamics by NOTCH1 and NRG1 defines the building plan for trabeculation. *Nature* **557**, 439-445. doi:10.1038/s41586-018-0110-6

Feldser, D., Agani, F., Iyer, N. V., Pak, B., Ferreira, G. and Semenza, G. L. (1999). Reciprocal positive regulation of hypoxia-inducible factor 1alpha and insulin-like growth factor 2. *Cancer Res.* **59**, 3915-3918.

Feng, S., Fragiadaki, M., Souilhol, C., Ridger, V. and Evans, P. C. (2017). Response by Feng et al. to letter regarding article, "Mechanical Activation of Hypoxia-Inducible Factor 1alpha Drives Endothelial Dysfunction at Atheroprone Sites". *Arterioscler. Thromb. Vasc. Biol.* **37**, e199-e200. doi:10.1161/ATVBAHA.117.310341

George, R. M. and Firulli, A. B. (2021). Deletion of a Hand1 lncRNA-containing septum transversum enhancer alters lncRNA expression but is not required for Hand1 expression. *J. Cardiovasc. Dev. Dis.* **8**, 50. doi:10.3390/jcdd8050050

Goddard, L. M., Duchemin, A.-L., Ramalingan, H., Wu, B., Chen, M., Bamezai, S., Yang, J., Li, L., Morley, M. P., Wang, T. et al. (2017). Hemodynamic forces sculpt developing heart valves through a KLF2-WNT9B paracrine signaling axis. *Dev. Cell* **43**, 274-289.e275. doi:10.1016/j.devcel.2017.09.023

Grego-Bessa, J., Luna-Zurita, L., del Monte, G., Bolós, V., Melgar, P., Arandilla, A., Garratt, A. N., Zang, H., Mukouyama, Y.-S., Chen, H. et al. (2007). Notch signaling is essential for ventricular chamber development. *Dev. Cell* **12**, 415-429. doi:10.1016/j.devcel.2006.12.011

Haack, T. and Abdelilah-Seyfried, S. (2016). The force within: endocardial development, mechanotransduction and signalling during cardiac morphogenesis. *Development* **143**, 373-386. doi:10.1242/dev.131425

Hao, Y., Hao, S., Andersen-Nissen, E., Mauck, W. M., III, Zheng, S., Butler, A., Lee, M. J., Wilk, A. J., Darby, C., Zager, M. et al. (2021). Integrated analysis of multimodal single-cell data. *Cell* **184**, 3573-3587.e3529. doi:10.1016/j.cell.2021.04.048

Harris, L. K. and Westwood, M. (2012). Biology and significance of signalling pathways activated by IGF-II. *Growth Factors* **30**, 1-12. doi:10.3109/08977194.2011.640325

Helker, C. S. M., Eberlein, J., Wilhelm, K., Sugino, T., Malchow, J., Schuermann, A., Baumeister, S., Kwon, H.-B., Maischein, H.-M., Potente, M. et al. (2020). Apelin signaling drives vascular endothelial cells toward a pro-angiogenic state. *eLife* **9**, e55589. doi:10.7554/eLife.55589

Huddleson, J. P., Srinivasan, S., Ahmad, N. and Lingrel, J. B. (2004). Fluid shear stress induces endothelial KLF2 gene expression through a defined promoter region. *Biol. Chem.* **385**, 723-729. doi:10.1515/BC.2004.088

Ivins, S., Chappell, J., Vernay, B., Suntharalingham, J., Martineau, A., Mohun, T. J. and Scambler, P. J. (2015). The CXCL12/CXCR4 axis plays a critical role in coronary artery development. *Dev. Cell* **33**, 455-468. doi:10.1016/j.devcel.2015.03.026

Kawanami, D., Mahabeleshwar, G. H., Lin, Z., Atkins, G. B., Hamik, A., Haldar, S. M., Maemura, K., Lamanna, J. C. and Jain, M. K. (2009). Kruppel-like factor 2 inhibits hypoxia-inducible factor 1α expression and function in the endothelium. *J. Biol. Chem.* **284**, 20522-20530. doi:10.1074/jbc.M109.025346

Kleaveland, B., Zheng, X., Liu, J. J., Blum, Y., Tung, J. J., Zou, Z., Sweeney, S. M., Chen, M., Guo, L., Lu, M.-M. et al. (2009). Regulation of cardiovascular development and integrity by the heart of glass-cerebral cavernous malformation protein pathway. *Nat. Med.* **15**, 169-176. doi:10.1038/nm.1918

Kuo, C. T., Veselits, M. L., Barton, K. P., Lu, M. M., Clendenin, C. and Leiden, J. M. (1997). The LKLF transcription factor is required for normal tunica media formation and blood vessel stabilization during murine embryogenesis. *Genes Dev.* **11**, 2996-3006. doi:10.1101/gad.11.22.2996

Kvon, E. Z., Zhu, Y., Kelman, G., Novak, C. S., Plajzer-Frick, I., Kato, M., Garvin, T. H., Pham, Q., Harrington, A. N., Hunter, R. D. et al. (2020). Comprehensive in vivo interrogation reveals phenotypic impact of human enhancer variants. *Cell* **180**, 1262-1271.e1215. doi:10.1016/j.cell.2020.02.031

Kwon, H.-B., Wang, S., Helker, C. S. M., Rasouli, S. J., Maischein, H.-M., Offermanns, S., Herzog, W. and Stainier, D. Y. R. (2016). In vivo modulation of endothelial polarization by Apelin receptor signalling. *Nat. Commun.* **7**, 11805. doi:10.1038/ncomms11805

Laurent, F., Girdziusaite, A., Gamart, J., Barozzi, I., Osterwalder, M., Akiyama, J. A., Lincoln, J., Lopez-Rios, J., Visel, A., Zuniga, A. et al. (2017). HAND2 target gene regulatory networks control atrioventricular canal and cardiac valve development. *Cell Rep.* **19**, 1602-1613. doi:10.1016/j.celrep.2017.05.004

Lee, J. S., Yu, Q., Shin, J. T., Sebzda, E., Bertozzi, C., Chen, M., Mericko, P., Stadtfeld, M., Zhou, D., Cheng, L. et al. (2006). Klf2 is an essential regulator of vascular hemodynamic forces in vivo. *Dev. Cell* **11**, 845-857. doi:10.1016/j.devcel.2006.09.006

Li, X., Lu, Q., Peng, Y., Geng, F., Shao, X., Zhou, H., Cao, Y. and Zhang, R. (2020). Primary cilia mediate Klf2-dependant Notch activation in regenerating heart. *Protein Cell* **11**, 433-445. doi:10.1007/s13238-020-00695-w

Lu, L., Wu, D., Li, L. and Chen, L. (2017). Apelin/APJ system: a bifunctional target for cardiac hypertrophy. *Int. J. Cardiol.* **230**, 164-170. doi:10.1016/j.ijcard.2016.11.215

Lu, Y. W., Martino, N., Gerlach, B. D., Lamar, J. M., Vincent, P. A., Adam, A. P. and Schwarz, J. J. (2021). MEF2 (Myocyte Enhancer Factor 2) is essential for endothelial homeostasis and the atheroprotective gene expression program. *Arterioscler. Thromb. Vasc. Biol.* **41**, 1105-1123. doi:10.1161/ATVBAHA.120.314978

Ludwig, T., Eggenschwiler, J., Fisher, P., D'Ercole, A. J., Davenport, M. L. and Efstratiadis, A. (1996). Mouse mutants lacking the type 2 IGF receptor (IGF2R) are rescued from perinatal lethality in Igf2 and Igf1r null backgrounds. *Dev. Biol.* **177**, 517-535. doi:10.1006/dbio.1996.0182

Luxán, G., D'Amato, G., MacGrogan, D. and de la Pompa, J. L. (2016). Endocardial Notch signaling in cardiac development and disease. *Circ. Res.* **118**, e1-e18. doi:10.1161/CIRCRESAHA.115.305350

Masatsugu, K., Itoh, H., Chun, T.-H., Saito, T., Yamashita, J., Doi, K., Inoue, M., Sawada, N., Fukunaga, Y., Sakaguchi, S. et al. (2003). Shear stress attenuates endothelin and endothelin-converting enzyme expression through oxidative stress. *Regul. Pept.* **111**, 13-19. doi:10.1016/S0167-0115(02)00219-7

Morawietz, H., Talanow, R., Szibor, M., Rueckschloss, U., Schubert, A., Bartling, B., Darmer, D. and Holtz, J. (2000). Regulation of the endothelin system by shear stress in human endothelial cells. *J. Physiol.* **525**, 761-770. doi:10.1111/j.1469-7793.2000.00761.x

Morikawa, Y. and Cserjesi, P. (2008). Cardiac neural crest expression of Hand2 regulates outflow and second heart field development. *Circ. Res.* **103**, 1422-1429. doi:10.1161/CIRCRESAHA.108.180083

Morikawa, Y., D'Autréaux, F., Gershon, M. D. and Cserjesi, P. (2007). Hand2 determines the noradrenergic phenotype in the mouse sympathetic nervous system. *Dev. Biol.* **307**, 114-126. doi:10.1016/j.ydbio.2007.04.027

Mummenhoff, J., Houweling, A. C., Peters, T., Christoffels, V. M. and Rüther, U. (2001). Expression of Irx6 during mouse morphogenesis. *Mech. Dev.* **103**, 193-195. doi:10.1016/S0925-4773(01)00353-7

Muzumdar, M. D., Tasic, B., Miyamichi, K., Li, L. and Luo, L. (2007). A global double-fluorescent Cre reporter mouse. *Genesis* **45**, 593-605. doi:10.1002/dvg.20335

Nigro, P., Abe, J.-I. and Berk, B. C. (2011). Flow shear stress and atherosclerosis: a matter of site specificity. *Antioxid Redox Signal.* **15**, 1405-1414. doi:10.1089/ars.2010.3679

Osterwalder, M., Tran, T., Hunter, R. D., Meky, E. M., von Maydell, K., Harrington, A. N., Godoy, J., Novak, C. S., Plajzer-Frick, I., Zhu, Y. et al. (2022). Characterization of mammalian in vivo enhancers using mouse transgenesis and CRISPR genome editing. In *Craniofacial Development Methods in Molecular Biology* (ed. J. M. Walker) pp. 147-186. Humana Press.

Parmar, K. M., Larman, H. B., Dai, G., Zhang, Y., Wang, E. T., Moorthy, S. N., Kratz, J. R., Lin, Z., Jain, M. K., Gimbrone, M. A., Jr et al. (2006). Integration of flow-dependent endothelial phenotypes by Kruppel-like factor 2. *J. Clin. Invest.* **116**, 49-58. doi:10.1172/JCI24787

Perez-Pinera, P., Berenson, J. R. and Deuel, T. F. (2008). Pleiotrophin, a multifunctional angiogenic factor: mechanisms and pathways in normal and pathological angiogenesis. *Curr. Opin Hematol.* **15**, 210-214. doi:10.1097/MOH.0b013e3282fdc69e

Phansalkar, R., Krieger, J., Zhao, M., Kolluru, S. S., Jones, R. C., Quake, S. R., Weissman, I., Bernstein, D., Winn, V. D., D'Amato, G. et al. (2021). Coronary blood vessels from distinct origins converge to equivalent states during mouse and human development. *eLife* **10**, e70246. doi:10.7554/eLife.70246.sa2

Pinto, A. R., Paolicelli, R., Salimova, E., Gospocic, J., Slonimsky, E., Bilbao-Cortes, D., Godwin, J. W. and Rosenthal, N. A. (2012). An abundant tissue macrophage population in the adult murine heart with a distinct alternatively-activated macrophage profile. *PLoS ONE* **7**, e36814. doi:10.1371/journal.pone.0036814

Razani, B., Engelman, J. A., Wang, X. B., Schubert, W., Zhang, X. L., Marks, C. B., Macaluso, F., Russell, R. G., Li, M., Pestell, R. G. et al. (2001). Caveolin-1 null mice are viable but show evidence of hyperproliferative and vascular abnormalities. *J. Biol. Chem.* **276**, 38121-38138. doi:10.1074/jbc.M105408200

Rhee, S., Paik, D. T., Yang, J. Y., Nagelberg, D., Williams, I., Tian, L., Roth, R., Chandy, M., Ban, J., Belbachir, N. et al. (2021). Endocardial/endothelial angiocrines regulate cardiomyocyte development and maturation and induce features of ventricular non-compaction. *Eur. Heart J.* **42**, 4264-4276. doi:10.1101/2020.07.25.220301

Robinson, A. S., Materna, S. C., Barnes, R. M., De Val, S., Xu, S.-M. and Black, B. L. (2014). An arterial-specific enhancer of the human endothelin converting enzyme 1 (ECE1) gene is synergistically activated by Sox17, FoxC2, and Etv2. *Dev. Biol.* **395**, 379-389. doi:10.1016/j.ydbio.2014.08.027

Sandovici, I., Georgopoulou, A., Pérez-García, V., Hufnagel, A., López-Tello, J., Lam, B. Y. H., Schiefer, S. N., Gaudreau, C., Santos, F., Hoelle, K. et al. (2022). The imprinted Igf2-Igf2r axis is critical for matching placental microvasculature expansion to fetal growth. *Dev. Cell* **57**, 63-79.e68. doi:10.1016/j.devcel.2021.12.005

Sangwung, P., Zhou, G., Nayak, L., Chan, E. R., Kumar, S., Kang, D.-W., Zhang, R., Liao, X., Lu, Y., Sugi, K. et al. (2017). KLF2 and KLF4 control endothelial identity and vascular integrity. *JCI Insight* **2**, e91700. doi:10.1172/jci.insight.91700

Seya, D., Ihara, D., Shirai, M., Kawamura, T., Watanabe, Y. and Nakagawa, O. (2021). A role of Hey2 transcription factor for right ventricle development through regulation of Tbx2-Mycn pathway during cardiac morphogenesis. *Dev. Growth Differ.* **63**, 82-92. doi:10.1111/dgd.12707

Sharma, B., Chang, A. and Red-Horse, K. (2017). Coronary artery development: progenitor cells and differentiation pathways. *Annu. Rev. Physiol.* **79**, 1-19. doi:10.1146/annurev-physiol-022516-033953

Shen, H., Cavallero, S., Estrada, K. D., Sandovici, I., Kumar, S. R., Makita, T., Lien, C.-L., Constancia, M. and Sucov, H. M. (2015). Extracardiac control of embryonic cardiomyocyte proliferation and ventricular wall expansion. *Cardiovasc. Res.* **105**, 271-278. doi:10.1093/cvr/cvu269

VanDusen, N. J., Casanovas, J., Vincentz, J. W., Firulli, B. A., Osterwalder, M., Lopez-Rios, J., Zeller, R., Zhou, B., Grego-Bessa, J., De La Pompa, J. L. et al. (2014a). Hand2 is an essential regulator for two Notch-dependent functions within the embryonic endocardium. *Cell Rep.* **9**, 2071-2083. doi:10.1016/j.celrep.2014.11.021

VanDusen, N. J., Vincentz, J. W., Firulli, B. A., Howard, M. J., Rubart, M. and Firulli, A. B. (2014b). Loss of Hand2 in a population of Periostin lineage cells results in pronounced bradycardia and neonatal death. *Dev. Biol.* **388**, 149-158. doi:10.1016/j.ydbio.2014.02.010

Vincentz, J. W., Casasnovas, J. J., Barnes, R. M., Que, J., Clouthier, D. E., Wang, J. and Firulli, A. B. (2016). Exclusion of Dlx5/6 expression from the distal-most mandibular arches enables BMP-mediated specification of the distal cap. *Proc. Natl. Acad. Sci. USA* **113**, 7563-7568. doi:10.1073/pnas.1603930113

Vincentz, J. W., Firulli, B. A., Toolan, K. P., Arking, D. E., Sotoodehnia, N., Wan, J., Chen, P.-S., de Gier-de Vries, C., Christoffels, V. M., Rubart-von der Lohe, M. et al. (2019). Variation in a left ventricle-specific Hand1 enhancer impairs GATA transcription factor binding and disrupts conduction system development and function. *Circ. Res.* **125**, 575-589. doi:10.1161/CIRCRESAHA.119.315313

Wang, Y., Wu, B., Chamberlain, A. A., Lui, W., Koirala, P., Susztak, K., Klein, D., Taylor, V. and Zhou, B. (2013). Endocardial to myocardial notch-wnt-bmp axis

regulates early heart valve development. *PLoS ONE* **8**, e60244. doi:10.1371/journal.pone.0060244

Wang, K., Shen, H., Gan, P., Cavallero, S., Kumar, S. R., Lien, C.-L. and Sucov, H. M. (2019). Differential roles of insulin like growth factor 1 receptor and insulin receptor during embryonic heart development. *BMC Dev. Biol.* **19**, 5. doi:10.1186/s12861-019-0186-8

Wang, Y., Lu, P., Jiang, L., Wu, B. and Zhou, B. (2020). Control of sinus venous valve and sinoatrial node development by endocardial NOTCH1. *Cardiovasc. Res.* **116**, 1473-1486. doi:10.1093/cvr/cvz249

Wani, M. A., Means, R. T., Jr and Lingrel, J. B. (1998). Loss of LKLF function results in embryonic lethality in mice. *Transgenic Res.* **7**, 229-238. doi:10.1023/A:1008809809843

Wu, B., Zhang, Z., Lui, W., Chen, X., Wang, Y., Chamberlain, A. A., Moreno-Rodriguez, R. A., Markwald, R. R., O'Rourke, B. P., Sharp, D. J. et al. (2012). Endocardial cells form the coronary arteries by angiogenesis through myocardial-endocardial VEGF signaling. *Cell* **151**, 1083-1096. doi:10.1016/j.cell.2012.10.023

Zhang, H., Pu, W., Li, G., Huang, X., He, L., Tian, X., Liu, Q., Zhang, L., Wu, S. M., Sucov, H. M. et al. (2016). Endocardium minimally contributes to coronary endothelium in the embryonic ventricular free walls. *Circ. Res.* **118**, 1880-1893. doi:10.1161/CIRCRESAHA.116.308749

Zheng, G. X. Y., Terry, J. M., Belgrader, P., Ryvkin, P., Bent, Z. W., Wilson, R., Ziraldo, S. B., Wheeler, T. D., McDermott, G. P., Zhu, J. et al. (2017). Massively parallel digital transcriptional profiling of single cells. *Nat. Commun.* **8**, 14049. doi:10.1038/ncomms14049

Zhou, Z., Tang, A. T., Wong, W.-Y., Bamezai, S., Goddard, L. M., Shenkar, R., Zhou, S., Yang, J., Wright, A. C., Foley, M. et al. (2016). Cerebral cavernous malformations arise from endothelial gain of MEKK3-KLF2/4 signalling. *Nature* **532**, 122-126. doi:10.1038/nature17178